the presence of appreciable amounts of circulating free FGF because FGF seems to be released into the extracellular matrix, where it accumulates and is internalized by cells. The presence of FGF bound to soluble heparan sulfate in the blood is also plausible. O. Saksela, D. Moscatelli, A. Sommer, D. B. Rifkin, *J. Cell Biol.* **107**, 743 (1988); D. Moscatelli, *ibid.*, p. 753; Y. Sato and D. Rifkin, *ibid.*, p. 1199; P. L. McNeil, L. Muthukrishnan, E. Warder, P. A. D'Amore, *ibid.* **109**, 811 (1989); O. Saksela and D. Rifkin, *ibid.* **110**, 767 (1990); R. Flaumenhaft, D. Moscatelli, D. B. Rifkin, *ibid.* **111**, 1651 (1990); D. Moscatelli, *J. Cell. Physiol.* **131**, 123 (1987); M. Kan *et al.*, *Proc. Natl. Acad. Sci. U.S.A.* **86**, 7432 (1989); D. Moscatelli, R. Flaumenhaft, O. Saksela, D. Rifkin, *Proceedings of the Conference on the Fibroblast Growth Factor Family*, La Jolla, CA, 16 to 18 January 1991 (New York Academy of Science, New York, 1991); D. Rifkin, *ibid.*

5. J. Vane, *Nature* **348**, 673 (1990).
6. K. Aisaka, S. S. Gross, O. W. Griffith, R. Levi, *Biochem. Biophys. Res. Commun.* **160**, 881 (1989); B. Mayer, K. Schmidt, P. Humbert, E. Böme, *ibid.* **164**, 678 (1989).
7. A. Pandiella, M. Magni, J. Meldolesi, *ibid.* **163**, 1325 (1989).
8. Human recombinant bFGF (provided by Farmitalia-Carlo Erba, Milan, Italy), did not elicit any appreciable reaction in toxicology studies. The aFGF was prepared as described [D. L. Linemeyer *et al.*, *Biotechnology* **5**, 960 (1987)], except we did not perform HPLC chromatography. Amino acid compositions of aFGF determined by amino acid analysis and deduced from the aFGF sequence, respectively, were as follows: Asp and Asn, 14.52, 15; Thr, 8.02, 8; Ser, 9.87, 10; Glu and Gln, 13.81, 15; Gly, 12.94, 13; Ala, 4.53, 4; Val, 5.20, 5; Met, 2.22, 2; Ile, 5.01, 5; Leu, 16.52, 17; Tyr, 7.88, 8; Lys, 11.00, 11; His, 5.05, 5; Arg, 6.32, 6; Pro, not determined, 8; Cys, not determined, 3; and Trp, not determined, 1. Wistar rats (160 to 200 g) of both sexes were anesthetized by intraperitoneal injection of 3 ml of a mixture per kilogram of body mass; the mixture consisted of ketamine hydrochloride (25 mg/ml), atropine (0.1 mg/ml), and Valium (2 mg/ml). For arterial blood pressure measurements, the common femoral artery was cannulated, and the catheter was moved into the abdominal aorta. The pressure was recorded on a monitor connected to the catheter by a pressure transducer. Pressure values at intervals of 1.6 s were averaged manually and digitized for computer analysis and graphing. FGF was injected into the external jugular vein in a single bolus (50 μl) in PBS with heparin (0.1 mg/ml) (PBS-heparin), except where indicated. Similar results to those of Fig. 1 were obtained when the injection was carried out in the contralateral common femoral artery or when the injection volume was brought up to 500 μl. New Zealand white rabbits (2 to 3.5 kg) of both sexes were sedated with 10 mg of ketamine hydrochloride (per kilogram of body mass) given through the ear marginal vein. Anesthesia was maintained with 1 to 3% halothane and a mixture of N_2O:O_2 (3:1). The FGF was injected in the contralateral femoral vein in a single 500 μl bolus in PBS-heparin.
9. P. Cuevas *et al.*, unpublished data.
10. T. K. Rosengart, J. P. Kuperschmid, T. Maciag, R. Clark, *Circ. Res.* **64**, 227 (1989). We calculated the maximum amount of FGF in the blood in a 1-min injection according to the equation:

$$F = -(K_2/K_1)(1 - e^{K_1 t}) + K_3$$

F, the total amount of FGF in the blood at time t; K_2, the FGF injection rate; K_1, the FGF distribution constant; and K_3, the FGF amount that remains in the blood after the distribution phase, which in the time range of our calculations can be assumed as constant.
11. G. Giménez-Gallego *et al.*, unpublished data.
12. Tertiary amines are able to occupy the choline-binding site contained in the COOH-terminus moiety (118 amino acids) of the autolysin of *S. pneumoniae*. The protein bound to DEAE-cellulose is eluted with 2% (w/v) choline but not by NaCl solutions up to 1.5 M. J. M. Sanz, R. López, J. L. García, *FEBS Lett.* **232**, 308 (1990); J. M. Sánchez-Puelles, J. M. Sanz, J. L. García, E. García, *Gene* (Amsterdam) **89**, 69 (1990).
13. D. D. Rees, R. M. J. Palmer, S. Moncada, *Proc. Natl. Acad. Sci. U.S.A.* **86**, 3375 (1989).
14. J. M. Fukuto, K. S. Wood, R. E. Byrns, L. J. Ignarro, *Biochem. Biophys. Res. Commun.* **168**, 458 (1990).
15. M. T. Nelson, Y. Huang, J. E. Brayden, J. Hescheler, B. Standen, *Nature* **344**, 770 (1990).
16. U. Quast and N. S. Cook, *Trends Pharmacol. Sci* **10**, 431 (1989).
17. We sedated New Zealand white rabbits (2 to 3.5 kg) with ketamine hydrochloride and implanted a catheter near the bifurcation of the abdominal aorta through the left common carotid artery for the injection of FGF and contrast media to make the arteries opaque. Automatic injection of contrast media (3 ml total at 1 ml/s) was electronically synchronized with the digital vascular imaging equipment. The angiographies were obtained 5 s after the onset of injection. FGF was injected in 500 μl of PBS-heparin.
18. Mean cross-sectional increase of large and medium size arteries after FGF injection (Fig. 3) was estimated at 41%.
19. T. Imamura *et al.*, *Science* **249**, 1567 (1990).
20. The decrease in blood pressure induced in anesthetized rabbits (*8*) by different amounts (micrograms of protein per animal) of native aFGF and the modified protein, respectively, were as follows: 1.4 μg of protein, 8.6 and 6.5 mmHg; 5.4 μg of protein, 17.8 and 15.4 mmHg; 10.7 μg of protein, 21.1 and 25.7 mmHg; and 21.4 μg of protein, 23.7 and 26.3 mmHg.
21. All animals were kept under the care of the vivarium staff and treated according to protocols approved by our institutional animal research committee. We thank R. Guillemin, J. M. Ramírez, and M. Nieto-Sampedro for comments; and B. Cuevas and A. Crespo for technical assistance. Partially supported by the Dirección General de Investigación Científica y Técnica.

20 May 1991; accepted 12 August 1991

DNA Bending by Fos and Jun: The Flexible Hinge Model

TOM K. KERPPOLA AND TOM CURRAN*

DNA bending is essential for the assembly of multiprotein complexes that contact several DNA sequence elements. An approach based on phasing analysis was developed that allows determination of both the directed DNA bend angle and the orientation of DNA bending. This technique has been applied to the analysis of DNA bending by the transcription regulatory proteins Fos and Jun. Complexes that contained different combinations of full-length and truncated Fos and Jun induced DNA bends of different magnitudes and orientations. The DNA bends induced by the individual proteins were determined on the basis of a quantitative model for DNA bending by dimeric complexes. This information was used to visualize the consequences of DNA bending by Fos and Jun for the structures of Fos-Jun-DNA and Jun-DNA complexes.

EUKARYOTIC GENE TRANSCRIPTION IS modulated by combinatorial interactions among sequence-specific DNA binding proteins (*1*). For interactions to occur between proteins bound to separate sequence elements, the DNA helix must often be distorted. Protein-induced DNA bending can participate in the regulation of transcription by facilitating assembly of initiation complexes (*2*). Thus, it is important to determine the orientation and magnitude of DNA bends induced by transcriptional regulatory proteins.

The proto-oncogenes c-*fos* and c-*jun* encode proteins that are members of the bZIP family of DNA binding proteins, which bind DNA as homo- or heterodimeric complexes (*3*). Dimerization is mediated by a leucine zipper interaction, and DNA binding requires an adjacent region that contains a high density of basic amino acids (*4*). This basic DNA binding domain adopts an α-helical structure upon binding to DNA (*5*). Models of the DNA binding complexes of bZIP proteins assume that the DNA binding domain interacts with a straight B-form DNA (B-DNA) recognition site (*6, 7*). However, contacts between a straight α helix and the major groove of straight B-DNA are limited to a maximum of 12 contiguous amino acids, which can contact a maximum of 5 bp on DNA. In contrast, the basic region extends over 20 residues, and the DNA contact regions for proteins in the bZIP family range between 12 and 16 bp (*8*). Thus, the basic region α helix or the DNA recognition site or both must be bent or distorted to allow for the observed regions of contact between the molecules.

Procedures have been developed to investigate protein-induced DNA bending that rely on the anomalous electrophoretic mobilities of bent DNA fragments (*9, 10*). Using these methods, we demonstrated that Fos-Jun heterodimers and Jun homodimers induce bends in opposite orientations and that complexes composed of peptides encompassing the dimerization and DNA binding domains bend DNA in the same

Department of Molecular Oncology and Virology, Roche Institute of Molecular Biology, Nutley, NJ 07110.

*To whom correspondence should be addressed.

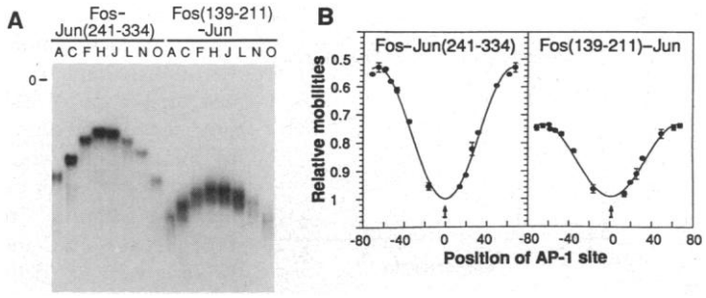

Fig. 1. Circular permutation analysis of protein-induced DNA flexure. (**A**) Electrophoretic mobility shift analysis of Fos-Jun (241-334) and Fos (139-211)-Jun heterodimers (*12*) bound to circularly permuted probes. The protein dimers were incubated with probes that contained an AP-1 site at different positions relative to the ends of the fragment (*11*). All probes were 133 bp in length and contained different circular permutations of the same sequence. The complexes were analyzed by polyacrylamide gel electrophoresis (PAGE) (*11*). (**B**) The relative mobilities of Fos-Jun(241-334) and Fos(139-211)-Jun complexes shown as a function of the position of the AP-1 site. There was no significant variation in probe mobilities in the absence of protein binding. The relative mobilities represent the average from three independent experiments, and the SDs are shown as vertical bars. The maximum is shown by an arrow, and the SD of maxima from different experiments is shown by a bar at the base of the arrow. The points are connected by the best fit of a cosine function (*14*).

orientations as the full-length proteins but induce smaller DNA bend angles (*11*). However, on the basis of these results, it was not possible to determine whether the opposite DNA bending properties were inherent to Fos and Jun or caused by a difference between hetero- and homodimeric complexes. To determine the effect of each protein and peptide on DNA bending, we have used a new quantitative approach to measure the orientation and magnitude of DNA bends induced by various combinations of Fos and Jun proteins and peptides.

The standard method for investigation of distortions in DNA structure, circular permutation analysis, is based on the position-dependent effect of DNA distortions on the electrophoretic mobilities of DNA fragments (*9*). When a distortion such as a bend is located at the center of a DNA fragment, the mobility of the fragment is retarded relative to that of a fragment of identical size that has the distortion at one end. Circular permutation analysis does not specifically detect DNA bends, because the method is also sensitive to other distortions in DNA structure, such as locations of increased DNA flexibility. Therefore, structures that cause a mobility variation in circular permutation analysis should be referred to as locations of DNA flexure, and the apparent DNA bend angle should be designated the DNA flexure angle. Circular permutation analysis of Fos-Jun(241-334) and Fos(139-211)-Jun heterodimers [for nomenclature, see (*12*)] demonstrated that both complexes induced distortions in DNA structure (Fig. 1). We have extended previous methods (*13*) for measurement of the DNA flexure angle (α_F) (*14*) to determine the DNA flexure angles induced by various combinations of Fos and Jun proteins and peptides (Table 1). These flexure angles are similar in magnitude to those induced by various prokaryotic DNA bending proteins (*13*).

Phasing analysis provides a specific method for the identification and analysis of DNA bends and is based on the phase-dependent interaction between a protein-induced DNA bend and an intrinsic DNA bend located on the same DNA fragment (*10, 11*). Two in-phase bends cooperate to increase the overall bend angle, whereas out-of-phase bends counteract each other to reduce the overall bend angle. Phasing analysis therefore allows one to discriminate between directed DNA bends and other distortions in DNA structure as well as to determine the orientation of DNA bends relative to the known orientation of intrinsic DNA bends containing phased A:T tracts. A critical difference between the phasing analysis performed here and phase-sensitive detection methods used in previous studies (*10*) is that here the protein binding site for Fos and Jun and the intrinsic DNA bend are directly abutting. As a consequence, DNA fragments that contain adjoining protein-induced and intrinsic bends can be approximated to contain a single bend, the orientation and magnitude of which represent the net sum of the protein-induced and intrinsic DNA bends.

Phasing analysis of Fos-Jun(241-334) and Fos(139-211)-Jun heterodimers demonstrated that Fos-Jun(241-334) induced a larger mobility variation than any of the

Table 1. DNA flexure and bending by dimeric complexes of different combinations of Fos and Jun proteins and peptides (*12*). The mobility anomaly is the ratio between the slowest and fastest migrating complexes (*13*). The DNA flexure angle was determined from the amplitude of the circular permutation function (*14*). The directed bend angle was determined from the amplitude of the phasing function (*16*). The orientation of bending was determined as described (*11*) and is expressed as an angle relative to the major groove–minor groove axis at the center of the AP-1 site. The orientation of intrinsic DNA bending toward the minor groove at the center of the A:T tract (*10*) was used as a standard and defined as 0°. The values represent averages and SDs derived from multiple independent experiments. Where no SD is given, the number of experiments was insufficient to give a meaningful SD. The DNA bend angles and orientations predicted on the basis of the independent DNA bends model were calculated as described in Fig. 3. The SDs of the predicted values were determined by propagation of errors. NA = not applicable.

Protein dimers	Circular permutation analysis			Phasing analysis			Independent bends model	
	Mobility anomaly (μ_{Max}/μ_{Min})	Circular permutation amplitude (A_{CP})	Flexure angle (α_F)	Phasing amplitude (A_{PH})	Directed bend angle (α_B)	Bend orientation (β_B)	Directed bend angle (α_B')	Bend orientation (β_B')
Fos-Jun	0.68 ± 0.01	0.35 ± 0.02	94 ± 3	0.24 ± 0.01	23.2 ± 1.4	333 ± 18	23.8 ± 1.6	329 ± 7
Jun-Jun	0.77 ± 0.01	0.25 ± 0.02	79 ± 3	0.28 ± 0.01	26.9 ± 0.6	124 ± 3	28.4 ± 2.0	127 ± 6
Fos(139-211)-Jun(241-334)	0.87 ± 0.01	0.14 ± 0.01	57 ± 3	0.12 ± 0.00	11.7 ± 0.2	319 ± 2	11.4 ± 0.1	308 ± 1
Jun(241-334)-Jun(241-334)	0.89 ± 0.01	0.12 ± 0.01	53 ± 1	0.12 ± 0.00	11.8 ± 0.4	128 ± 2	10.3 ± 0.1	123 ± 1
Fos-Jun(241-334)	0.55 ± 0.02	0.48 ± 0.02	111 ± 3	0.35 ± 0.01	33.3 ± 0.8	322 ± 1	32.5 ± 1.9	324 ± 6
Fos(139-211)-Jun	0.75 ± 0.01	0.27 ± 0.01	81 ± 2	0.03 ± 0.00	3.2 ± 0.4	261 ± 6	2.3 ± 0.1	304 ± 4
Fos(118-211)-Jun(225-334)	0.90 ± 0.02	0.11 ± 0.02	52 ± 4	0.10 ± 0.01	10.3 ± 0.5	329 ± 6	9.6	310
Jun(225-334)-Jun(225-334)	0.91 ± 0.01	0.10 ± 0.01	49 ± 1	0.14	13.5	123	11.6	128
Fos-Jun(225-334)	0.59	0.45	107	0.35	33.3	321	31.8	323
Fos(118-211)-Jun	0.74	0.28	83	0.03	2.8	241	1.4	338
Probes	0.98 ± 0.01	0.01 ± 0.02	NA	0.06 ± 0.00	NA	NA	NA	NA

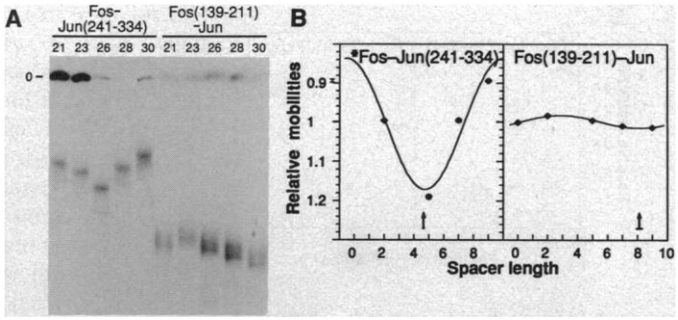

Fig. 2. Phasing analysis of protein-induced DNA bending. (**A**) Electrophoretic mobility shift analysis of Fos-Jun(241-334) and Fos(139-211)-Jun heterodimers (*12*) bound to phasing analysis probes. The protein dimers indicated above the lanes were prepared by association of purified proteins and were incubated with probes that contained an AP-1 site separated by a variable length spacer from an intrinsic DNA bend (*11*). The numbers above the lanes indicate the distance between the centers of the AP-1 site and the intrinsic DNA bend in base pairs. With the exception of the variable spacer length, all probes were of the same size (350 to 360 bp) and contained the same sequences. The complexes were analyzed by PAGE (*11*). (**B**) The relative mobilities of Fos-Jun(241-334) and Fos(139-211)-Jun complexes shown as a function of spacer length. The complex mobilities were corrected for variations in probe mobilities, normalized to the average mobility of all complexes, and plotted as a function of spacer length. The relative mobilities represent the average from three independent experiments. SDs and maxima are represented as in Fig. 1. The points are connected by the best fit of a cosine function (*16*).

other complexes tested, whereas Fos(139-211)-Jun caused little variation in complex mobilities (Fig. 2). This result is in contrast to the results from circular permutation analysis, in which both complexes induced similar variations in mobility (Fig. 1). Because phasing analysis specifically detects DNA bends, whereas circular permutation analysis is affected by other distortions in DNA structure, a likely interpretation of these results is that Fos-Jun(241-334) induced a directed DNA bend, whereas Fos(139-211)-Jun induced little or no net DNA bending but increased the flexibility of the AP-1 site (*15*). To determine the magnitude of the DNA bend angle, we derived a relation between the directed DNA bend angle (α_B) and the amplitude of the phasing function (A_{PH}) that allows determination of the directed DNA bend angle independent of other contributions to DNA flexure (*16*). On the basis of this relation, we determined the directed DNA bend angles for various combinations of Fos and Jun proteins and peptides (Table 1).

The DNA bend angles and orientations induced by Fos and Jun complexes (Table 1) demonstrated that neither the bend angle nor the bend orientation was a simple function of the molecular mass, the charge, or the heterodimer versus homodimer nature of the complex. To explain the observed DNA bend angles and orientations, we developed a model for DNA bending by Fos and Jun. In this model, each subunit of the dimeric complex induces an independent DNA bend of characteristic orientation and magnitude, and the overall DNA bend angle reflects the sum of the bends contributed by each subunit. A specific observation that can be explained by this model, but not by several other models we considered, was the absence of a directed DNA bend in the Fos(139-211)-Jun complex. Because other complexes that contained Fos(139-211) or Jun did induce DNA bending, and because the Fos(139-211)-Jun heterodimer induced DNA flexure, the simplest interpretation is that the DNA bends induced by Fos(139-211) and Jun counteract each other. The orientation of the small remaining bend angle was perpendicular to the bends induced by Fos-Jun heterodimers and Jun homodimers, which is consistent with cancellation of the major vector components of DNA bending in this complex. We designate this structure that contains two bends of opposite orientations a DNA "jog."

The DNA bend angles and orientations induced by individual Fos and Jun subunits were determined on the basis of a quantitative model that finds the best fit of the sums of subunit bends to the observed dimer bends (Fig. 3). This quantitative model could accurately reproduce the DNA bend angles and orientations of all of the complexes (Table 1). To further test this model, we omitted individual complexes and determined the bend angle and orientation predicted for each complex on the basis of the remaining complexes. The DNA bend angle and orientation of each complex could be predicted on the basis of the bends induced by the remaining complexes, with a maximum error of 5° in bend angle and 30° in bend orientation [the orientations of Fos(139-211)-Jun and Fos(118-211)-Jun bending were not defined because they did not induce DNA bend angles].

The DNA bend angles and bend orientations determined for the individual Fos and Jun proteins (Fig. 3B) provide information about the path of the DNA helix within the protein-DNA complex. We used molecular graphics to analyze the consequences of DNA bending for the structure of the protein-DNA complex. The DNA binding domains of Fos and Jun are predicted to be highly α-helical (*5*) and to contact the DNA helix within the major groove (*8, 17*). Therefore, we investigated how α-helical DNA binding domains would fit into the major groove of a bent DNA helix (Fig. 4). The predictions from the DNA structure analysis depart in several respects from other models for leucine zipper–basic region proteins (*6, 7*). Most obviously, the DNA helix is bent in both the Fos-Jun-DNA and Jun-DNA complexes. The opposite orientations of DNA bending induced by Fos and Jun suggest that their basic regions adopt different structures upon DNA binding. Fos bends DNA away from the dimer interface, causing the major groove to extend in a relatively linear fashion over the region of the recognition site (Fig. 4a). This DNA bend obviates the need to invoke a bend in the basic region α helix of Fos. Instead, the Fos basic region can extend as a contiguous α helix from the leucine zipper to the end of the basic region (Fig. 4b). The backbone dihedral angles of the invariant asparagine residue in Fos are within the normal range for residues within an α helix (Fig. 4c).

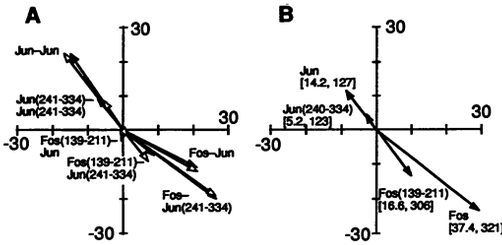

Fig. 3. Determination of DNA bend angles and orientations induced by individual Fos and Jun proteins and peptides based on the independent DNA bends model. (**A**) The DNA bends induced by various hetero- and homodimer complexes are represented as vectors, the lengths of which indicate the magnitude of the DNA bend angles and the directions of which indicate the orientation of bending at the center of the AP-1 site [closed arrows in (A)]. (**B**) We calculated the predicted DNA bends for each subunit [closed arrows in (B)] by finding the best fit of the predicted subunit bend vector sums [open arrows in (A)] to the dimer bend vector data [closed arrows in (A)]. The calculated DNA bend angle and orientation for each subunit is shown in brackets [α_B', β_B']. For simplicity, the DNA bend angles and orientations of only six different dimers composed of four individual proteins and peptides are shown. For the actual model, 13 different dimers composed of seven individual proteins were used in the initial calculation, and additional complexes were subsequently added. Therefore, the number of complexes was much larger than the number of independent variables in the model.

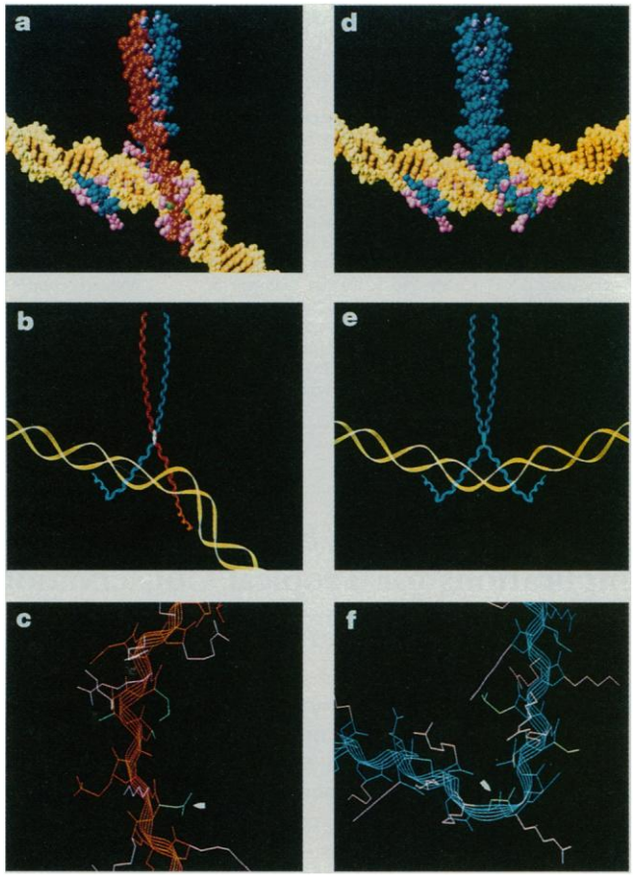

Fig. 4. Molecular graphics illustrations of the "flexible hinge" models of Fos(red)-Jun(blue) heterodimer (**a** through **c**) and Jun homodimer (**d** through **f**) complexes bound to the AP-1 recognition sequence (orange) (*24*). The leucine zipper (violet) was based on a standard coiled-coil conformation. The side chains of the basic residues within the DNA binding domain (magenta) are in a position where they can make electrostatic contacts with the phosphodiester backbone (yellow). The Cys, Ala, Ala, and Asn residues (green) in the DNA binding domain are conserved throughout the bZIP protein family. (a and d) Space-filling models show the close fit between the α helices and the major grooves of the bent DNA helices. (b and e) Backbone ribbon models show the Fos (red) DNA binding domain as a contiguous α helix, whereas the Jun (blue) DNA binding domain consists of two separate α-helical segments. (c and f) A close-up view of the geometry of the peptide backbone around the invariant asparagine residue (white arrow).

In contrast to Fos, Jun bends DNA toward the dimer interface, which requires distortion of the basic region α helix (Fig. 4d). It has been proposed that the basic region of bZIP proteins consists of two α-helical segments separated by a turn at an invariant asparagine residue (*6*). The curvature of the major groove in the bent DNA helix fits well with the angle between two α helices generated by an asparagine N cap in one of the two conserved conformations ($\psi = 100°$) (*18*) (Fig. 4e). However, because of the bend in the DNA helix, the geometry of the turn between the Jun α helices in this model is different from that suggested previously (Fig. 4f). The orientation of DNA bending induced by the Jun homodimer predicts that the dimer interface is displaced from the center of the recognition site (*19*). Consequently, although the core of the AP-1 recognition sequence is palindromic and the DNA binding domains of the Jun homodimer are predicted to be symmetric, the complex between the two is asymmetric. This result is consistent with mutational studies suggesting that the AP-1 site is recognized in an asymmetric manner (*20*).

Our results indicate that Fos and Jun induce directed DNA bending and an increase in flexibility of the AP-1 site (*15*). Both characteristics could contribute to transcription regulation by Fos and Jun.

Fos and Jun are induced in many cell types, and therefore their target gene specificity is likely to depend on the cellular context (*21*). The situation is complicated by the existence of several Fos- and Jun-related proteins that form dimers with similar DNA binding properties (*22*) and form heterodimers with several members of the CREB-ATF protein family (*23*). DNA binding by a specific bZIP dimer may induce a characteristic DNA conformation in target sequences and cause distinct transcriptional responses. Alternatively, because of flanking sequences or the presence of other DNA binding proteins, different target elements may favor distinct conformations that allow recognition by specific bZIP dimers. In either case, induction of independent DNA bends by each subunit in the complex provides a mechanism for the integration of separate signaling pathways.

REFERENCES AND NOTES

1. P. J. Mitchell and R. Tjian, *Science* **245**, 371 (1989).
2. F. Rojo *et al.*, *J. Mol. Biol.* **211**, 713 (1990); T. R. Hoover *et al.*, *Cell* **63**, 11 (1990); J. W. Gober and L. Shapiro, *Genes Dev.* **4**, 1494 (1990); S. S. Zinkel and D. M. Crothers, *J. Mol. Biol.* **219**, 201 (1991).
3. D. Bohmann *et al.*, *Science* **238**, 1386 (1987); F. J. Rauscher III *et al.*, *ibid.* **240**, 1010 (1988); T. Curran and B. R. Franza, Jr., *Cell* **55**, 305 (1988).
4. W. H. Landschulz *et al.*, *Science* **240**, 1759 (1988); T. Kouzarides and E. Ziff, *Nature* **336**, 646 (1988); W. H. Landschulz *et al.*, *Science* **243**, 1681 (1989); R. Turner and R. Tjian, *ibid.*, p. 1689; R. Gentz *et al.*, *ibid.*, p. 1695.
5. R. V. Talanian *et al.*, *Science* **249**, 769 (1990); L. Patel *et al.*, *Nature* **347**, 572 (1990); M. A. Weiss *et al.*, *ibid.*, p. 575.
6. C. R. Vinson *et al.*, *Science* **246**, 911 (1989).
7. K. T. O'Neil *et al.*, *ibid.* **249**, 774 (1990).
8. Y. Nakabeppu and D. Nathans, *EMBO J.* **8**, 3833 (1989); J. A. Nye and B. J. Graves, *Proc. Natl. Acad. Sci. U.S.A.* **87**, 3992 (1990); M. R. Gartenberg *et al.*, *ibid.*, p. 6034.
9. H.-M. Wu and D. M. Crothers, *Nature* **308**, 509 (1984).
10. S. S. Zinkel and D. M. Crothers, *ibid.* **328**, 178 (1987).
11. T. K. Kerppola and T. Curran, *Cell* **66**, 317 (1991).
12. Fos and Jun proteins and peptides were expressed in *Escherichia coli* as hexahistidine fusion proteins and purified to >90% homogeneity by nickel chelate affinity chromatography. Dimers were prepared by association of the appropriate proteins as described (*11*). Peptides are designated by residue numbers in parentheses. Thus, the designation Fos-Jun(225-334) refers to a dimer containing full-length Fos and a Jun peptide encompassing residues 225 to 334. The Fos(139-211), Fos(118-211), Jun(241-334), and Jun(225-334) peptides used here are identical to those described previously [C. Abate *et al.*, *Proc. Natl. Acad. Sci. U.S.A.* **87**, 1032 (1990); C. Abate *et al.*, *Mol. Cell. Biol.* **11**, 3624 (1991)]; however, because of an oversight, the residue numbers used in the original publications were incorrect and are revised here.
13. J. F. Thompson and A. Landy, *Nucleic Acids Res.* **16**, 9687 (1988).
14. To determine the DNA flexure angle, we calculated the best fit of a cosine function to the relative mobilities of circular permutation analysis complexes. The term "circular permutation function" refers to this best fit relation, and "circular permutation function amplitude" refers to the amplitude of this function. The circular permutation function amplitude is a more accurate measure of the mobility variation in circular permutation analysis than the traditionally used mobility anomaly (μ_M/μ_E) because it includes information from all of the probes used and it is not affected by the distance between the binding site and the closest restriction enzyme cleavage site. We have derived a relation between the circular permutation function amplitude (A_{CP}) and DNA flexure angle (α_F) from the dependence of electrophoretic mobility on end-to-end distance

$$\mu_M/\mu_E = \cos(\alpha/2) \quad (1)$$

(μ_M, mobility with the bend at the middle; μ_E, mobility with the bend at the end) (*13*). In practical terms, the relative electrophoretic mobilities are influenced by a number of factors, including temperature, gel composition, fragment length, and electrical field strength. To account for these factors we have introduced a coefficient k into the function:

$$\mu_M/\mu_E = \cos(k\alpha/2) \quad (2)$$

By normalizing the mobilities to $\mu_E = 1$ and substituting $\mu_M = 1 - A_{CP}$ and $\alpha = \alpha_F$, we obtain

$$A_{CP} = 1 - \cos(k\alpha_F/2) \quad (3)$$

To determine the value of k under our conditions, we used two sets of standards containing intrinsically bent DNA sequences. The first set of standards was provided by J. Thompson and A. Landy and contains from two to nine phased A:T tracts, each of which causes a bend of approximately 18°, inserted between tandem repeats of heterologous sequences (plasmids pJT170 − n; n = 2 to 9) (*13*). The mobility variation induced by these intrinsic bends followed a cosine function of the bend angle up to 140° (*13*). However, the lengths and sequences of this set of standards differed from those we used in the circular permutation analysis here. To correct for differences in lengths and sequences, we constructed

a second set of standards by inserting three phased A:T tracts at different positions adjacent to the AP-1 site in the circular permutation analysis plasmids (*11*). The value $k = 1.06$ was determined from the best fit of Eq. 3 to the circular permutation function amplitudes of the standard probes.

15. The directed DNA bend angles induced by all of the complexes we investigated were smaller than the DNA flexure angles (Table 1). This difference between the DNA bend angle and the DNA flexure angle was not a result of an underestimate of the DNA bend angle by phasing analysis because the ranking of the complexes by DNA flexure angle and DNA bend angle was different. In addition, some complexes that induced little or no directed DNA bending [for example, Fos(139-211)-Jun] caused DNA flexure. We suggest that the larger DNA flexure angle is caused by other structural distortions such as an increase in DNA flexibility.
16. To determine the directed DNA bend angle, we calculated the best fit of a cosine function to the relative mobilities of phasing analysis complexes. The term "phasing function" refers to this best fit relation, and "phasing function amplitude" refers to the amplitude of this function. We have derived the relation between the phasing function amplitude (A_{PH}) and the directed DNA bend angle (α_B) from the dependence of electrophoretic mobility on end-to-end distance (Eq. 2). The ratio between the mobilities of two fragments of identical lengths but with different bend angles α_1 and α_2 at the middle is

$$\mu_1/\mu_2 = \cos(k\alpha_1/2)/\cos(k\alpha_2/2) \quad (4)$$

Tandem DNA bends are additive when placed in phase and cancel almost perfectly when placed out of phase [P. J. Hagerman, *Biochemistry* **24**, 7033 (1985); H.-S. Koo *et al.*, *Nature* **320**, 501 (1986)]. In the case of phasing analysis, the relation between maximum mobility, μ_{Max}, when the two bends counteract each other ($\alpha_1 = \alpha_B - \alpha_C$), and minimum mobility, μ_{Min}, when the two bends cooperate ($\alpha_2 = \alpha_B + \alpha_C$), is therefore

$$\mu_{Max}/\mu_{Min} = \cos[k(\alpha_B - \alpha_C)/2]/\cos[k(\alpha_B + \alpha_C)/2] \quad (5)$$

which can be resolved with standard trigonometrical relations to give

$$\tan(k\alpha_B/2) = \frac{\mu_{Max}/\mu_{Min} - 1}{(\mu_{Max}/\mu_{Min} + 1)\tan(k\alpha_C/2)} \quad (6)$$

Because μ_{Max} and μ_{Min} cannot be directly determined, we substitute $\mu_{Max}/\mu_{Min} = (1 + A_{PH}/2)/(1 - A_{PH}/2)$ to obtain

$$\tan(k\alpha_B/2) = \frac{A_{PH}/2}{\tan(k\alpha_C/2)} \quad (7)$$

Because the mobilities of bent DNA fragments depend on the end-to-end distance up to a bend angle of approximately 140°, and because the angle of the reference bend in these experiments is 54°, this function is expected to be valid up to a bend angle of approximately 90°.

17. M. G. Oakley and P. B. Dervan, *Science* **248**, 847 (1990).
18. J. S. Richardson and D. C. Richardson, *ibid.* **240**, 1648 (1988).
19. The Jun homodimer bends DNA in an orientation that is rotated 56° relative to the major groove–minor groove axis at the center of the AP-1 site. Our data indicate that the Jun homodimer subunits induce equivalent and symmetrical DNA bends. If the dimer interface is centered over the major groove (*8, 17*), the Jun homodimer can only bend DNA in an orientation parallel with the major groove–minor groove axis at the dimer interface. Therefore, the Jun homodimer must be displaced by 1.5 bp in order to align the observed orientation of bending with the major groove–minor groove axis.
20. G. Risse *et al.*, *EMBO J.* **8**, 3825 (1989).
21. J. I. Morgan and T. Curran, *Annu. Rev. Neurosci.* **14**, 421 (1991).
22. Y. Nakabeppu *et al.*, *Cell* **55**, 907 (1988); D. R. Cohen *et al.*, *Genes Dev.* **3**, 173 (1989); M. Zerial *et al.*, *EMBO J.* **8**, 805 (1989).
23. T. Hai and T. Curran, *Proc. Natl. Acad. Sci. U.S.A.* **88**, 3720 (1991).
24. The structures of the Fos-Jun-DNA and Jun-DNA complexes predicted on the basis of the observed DNA trajectories were visualized with the SYBYL molecular graphics program. Since our data do not specify the distribution of the DNA bend among individual dinucleotides, we generated smooth bends by introducing equal wedges between each dinucleotide pair. Amino acid residues 136 to 200 in Fos and 254 to 318 in Jun were used to construct the models. These residues encompass the basic regions and leucine zippers of Fos and Jun, including the histidine residues at the COOH-terminal ends of the zippers that contribute to dimerization efficiency [D. R. Cohen and T. Cusran, *Oncogene* **5**, 929 (1990)]. The leucine zipper structure was modeled on the basis of standard coiled-coil conformation. Our data do not specify the orientation of Fos-Jun binding to the AP-1 site. However, in our model we favor the orientation in which Jun contacts the more stringently conserved half of the AP-1 site (*20*). The basic regions of Fos and Jun were modeled by starting with standard α helices and optimizing contacts with the major groove using both manual adjustments and local energy minimization programs (ANNEAL). The N cap in the Jun basic region was modeled on the basis of the conserved N cap geometry (*18*). Side chain conformations were not fully optimized. The atomic coordinates for this model will be provided on request.
25. We thank C. Cook for his assistance with the SYBYL molecular graphics program; C. Abate for providing Fos and Jun dimerization–DNA binding domain peptides for these experiments; and D. Nuss and C. Rosen for critical reading of the manuscript. T.K.K. is supported by a postdoctoral fellowship from The Helen Hay Whitney Foundation.

25 June 1991; accepted 9 September 1991

Genetic Mosaics in Strangler Fig Trees: Implications for Tropical Conservation

JAMES D. THOMSON,* E. A. HERRE, J. L. HAMRICK, J. L. STONE

Single trees of six species of strangler figs (*Ficus* spp., Moraceae) in Panama were found to be made up of multiple genotypes, presumably formed by the fusion of different individuals. The phenomenon is frequent enough that strangler fig populations will contain considerably more genetic variation than would be expected from the number of trees. How this cryptic variation affects populations depends on the flowering phenology of composite trees. If the genetically different portions of trees flower asynchronously, populations of pollinating wasps may be more resistant to low host population sizes than previously thought. If different portions flower synchronously, attempts to infer mating-system parameters from the parentage of fruit crops will be misleading. The fruiting of figs, which are considered a keystone species in tropical forests, is important for maintaining biodiversity but is also particularly susceptible to failure at small population sizes. It is therefore important to know both the number of trees and the number of genotypes in a population.

JANZEN (*1*) HAS MARSHALLED A COMpelling argument that figs (*Ficus* spp., Moraceae) possess sufficient biological peculiarities to render them fundamentally different from other tropical trees. Most of these distinctions arise from the fig's need for pollination by tiny, species-specific wasps (Agaonidae) that develop within the specialized inflorescences (*1–3*). The classical view [to which exceptions exist (*4*)] is that flowering and fruiting episodes are tightly synchronized: A tree releases a huge crop of pollen-bearing female wasps that must locate a conspecific tree that is at the proper (earlier) developmental stage to receive wasps; there, they can oviposit inside the inflorescences. Wasps of both sexes grow, pupate, and mate as the inflorescences develop; then the females leave to renew the cycle. This within-tree synchrony is coupled with between-tree asynchrony in flowering and fruiting, which is necessary to maintain populations both of pollinating wasps and, because some fig fruits are available all year, of fruit-eating vertebrates: "All the larger primates use figs heavily, as do procyonids, marsupials, guans, trumpeters, toucans, and many other birds . . . . Subtract figs from the ecosystem and one could expect to see it collapse" (*5*).

Figs are regarded as keystones (*5–8*) for conservation in many [if not all (*9*)] tropical forests, yet their flowering asynchrony renders them particularly vulnerable to forest reduction and fragmentation (*6, 10*). Although species of figs are numerous in most tropical forests, individuals are typically sparse (*1, 6*). Simulation models based on fig phenologies (*4, 11, 12*) suggest that about 100 trees may be necessary to maintain local populations of the wasps, leading to a proposal that 300 trees might be considered a minimum viable population size (*6*); wasps die within a few days if no tree is receptive when they are released, and fig

J. D. Thomson and J. L. Stone, Department of Ecology and Evolution, State University of New York, Stony Brook, NY 11794.
E. A. Herre, Smithsonian Tropical Research Institute, P. O. Box 2072, Balboa, Panama.
J. L. Hamrick, Departments of Botany and Genetics, Athens, GA 30602.